Fullerenes and Fullerides: Photoemission and Scanning Tunneling Microscopy Studies

JOHN H. WEAVER

Department of Materials Science and Chemical Engineering, University of Minnesota, Minneapolis, Minnesota 55455

Received December 16, 1991 (Revised Manuscript Received January 8, 1992)

Introduction

The discovery of carbon-cage fullerenes[1] and the development of procedures for producing sizable quantities of them[2] sparked intense scientific inquiry, as this issue attests. Critical to many of these studies is insight into the distribution of electronic states. Such insight is important for isolated fullerenes, for example, because the state distribution serves as a direct test of the symmetry or structure of the molecule and the ability of theory to describe it. The state distribution is important in understanding fullerites, the condensed form of fullerenes, because condensation introduces solid effects, and band formation then dictates the electrical properties and the optical properties, among other things. Studies of the electronic states have demonstrated that the fullerite is characterized by van der Waals bonding with limited valence-level broadening, increasing broadening for states above the Fermi level, E_F, and significant molecular character.

Investigations of the electronic states of compounds formed by mixing C_{60} with other species, notably the alkali and alkaline-earth fullerides, are critical because they show the way that C_{60} bonds to these atoms in the solid state. For example, experimental and theoretical investigations for K_3C_{60} have demonstrated electron transfer to the fullerene, occupation of the LUMO-derived band, and ionic compound formation, but relatively little modification of the fullerene. For the alkaline-earth fullerides, more covalent bonding was observed. For doping with iodine, a possible p-type dopant, there was very little charge transfer. In each case, a detailed investigation of the electronic states tests our ability to understand bonding and solid-state effects. The distribution of electronic states and their character near E_F are crucial for elucidating the mechanisms of superconductivity.

Additional insight into fullerene interactions come from spectroscopic studies of their bonding to surfaces. Since bonding reflects coupling of the surface to electrons of the molecule, the distribution of states and the extent of hybridization can be obtained by electronic structure studies. Such studies are critical for those interested in adsorption, thin film formation, and surface-moderated reactions.

For thin films of fullerenes, or other materials for that matter, many of the solid-state properties are dictated by their microstructures. For fullerene films, electronic structure investigations have made it possible to examine the effects of defect levels associated with grain boundaries and other states in the gap that would pin the Fermi level, as in conventional semiconductors. Investigations using scanning tunneling microscopy have made it possible to explore growth phenomena, surface structures, and the electronic states of the fullerenes.

This paper focuses on thin films of C_{60} and thin films of the alkali-metal fullerides and examines their electronic properties. The experimental techniques include photoemission and inverse photoemission because they reveal the distribution and character of the electronic states and related electron excitations, particularly π–π^* excitation features and collective resonances of the charge of a single molecule, i.e., molecular plasmons.[3-8] The nature of the band gap is discussed, and connections to optical properties are established. For the fullerides, it is possible to observe the disappearance of emission from the empty-state spectrum and the appearance of emission in the occupied-state spectrum.[7,8] Scanning tunneling microscopy reveals surface bonding of the fullerenes with GaAs and Si and the formation of multilayers on thin films.[9,10]

Experimental

Phase-pure powders of C_{60} were separated by toluene extraction and liquid chromatography from the soot produced by arc discharge of grpahite.[11] The fullerenes were sublimed from Ta boats heated to ~550 °C in ultrahigh vacuum, and they were condensed onto clean substrates, all while chamber pressures were maintained

John H. Weaver obtained a B.S. from the University of Missouri and a Ph.D. from Iowa State University, both in physics. He was with the Synchrotron Radiation Center at the University of Wisconsin from 1974 until 1982, when he joined the faculty of the University of Minnesota as head of the Electronic Materials Group. His interests include surface and interface phenomena for a wide range of materials systems.

(1) Kroto, H. W.; Heath, J. R.; O'Brien, S. C.; Curl, R. F.; Smalley, R. E. *Nature* **1985**, *318*, 162.
(2) Krätschmer, W.; Lamb, L. D.; Fostiropoulos, K.; Huffman, D. R. *Nature* **1990**, *347*, 354.
(3) Weaver, J. H.; Martins, J. L.; Komeda, T.; Chen, Y.; Troullier, N.; Ohno, T. R.; Kroll, G. H.; Haufler, R. E.; Smalley, R. E. *Phys. Rev. Lett.* **1991**, *66*, 1741. See also: Lichtenberger, D. L.; Nebesny, K. W.; Ray, C. D.; Huffman, D. R.; Lamb, L. D. *Chem. Phys. Lett.* **1991**, *176*, 203.
(4) Jost, M. B.; Troullier, N.; Poirier, D. M.; Martins, J. L.; Weaver, J. H.; Chibante, L. P. F.; Smalley, R. E. *Phys. Rev.* **1991**, *B44*, 1966.
(5) Martins, J. L.; Troullier, N.; Weaver, J. H. *Chem. Phys. Lett.* **1991**, *180*, 457.
(6) Benning, P. J.; Poirier, D. M.; Troullier, N.; Martins, J. L.; Weaver, J. H.; Haufler, R. E.; Chibante, L. P. F.; Smalley, R. E. *Phys. Rev.* **1991**, *B44*, 1962.
(7) Benning, P. J.; Martins, J. L.; Weaver, J. H.; Chibante, L. P. F.; Smalley, R. E. *Science* **1991**, *252*, 1417. Wertheim, G. K.; Rowe, J. E.; Buchanan, D. N. E.; Chaban, E. E.; Hebard, A. F.; Kortan, A. R.; Makhija, A. V.; Haddon, R. C. *Science* **1991**, *252*, 1419.
(8) Benning, P. J.; Poirier, D. M.; Ohno, T. R.; Chen, Y.; Jost, M. B.; Stepniak, F.; Kroll, G. H.; Weaver, J. H.; Fure, J.; Smalley, R. E. *Phys. Rev.*, in press.
(9) Li, Y. Z.; Patrin, J. C.; Chander, M.; Weaver, J. H.; Chibante, L. P. F.; Smalley, R. E. *Science* **1991**, *252*, 547.
(10) Li, Y. Z.; Chander, M.; Patrin, J. C.; Weaver, J. H.; Chibante, L. P. F.; Smalley, R. E. *Science* **1991**, *253*, 429.
(11) Haufler, R. E.; Conceicao, J.; Chibante, L. P. F.; Chai, Y.; Bryne, N. E.; Flanagan, S.; Haley, M. M.; O'Brien, S. C.; Pan, C.; Xiao, Z.; Billups, W. E.; Ciufoline, M. A.; Hauge, R. H.; Margrave, J. L.; Wilson, L. J.; Curl, R. F.; Smalley, R. E. *J. Phys. Chem.* **1990**, *94*, 8634.

0001-4842/92/0125-0143$03.00/0

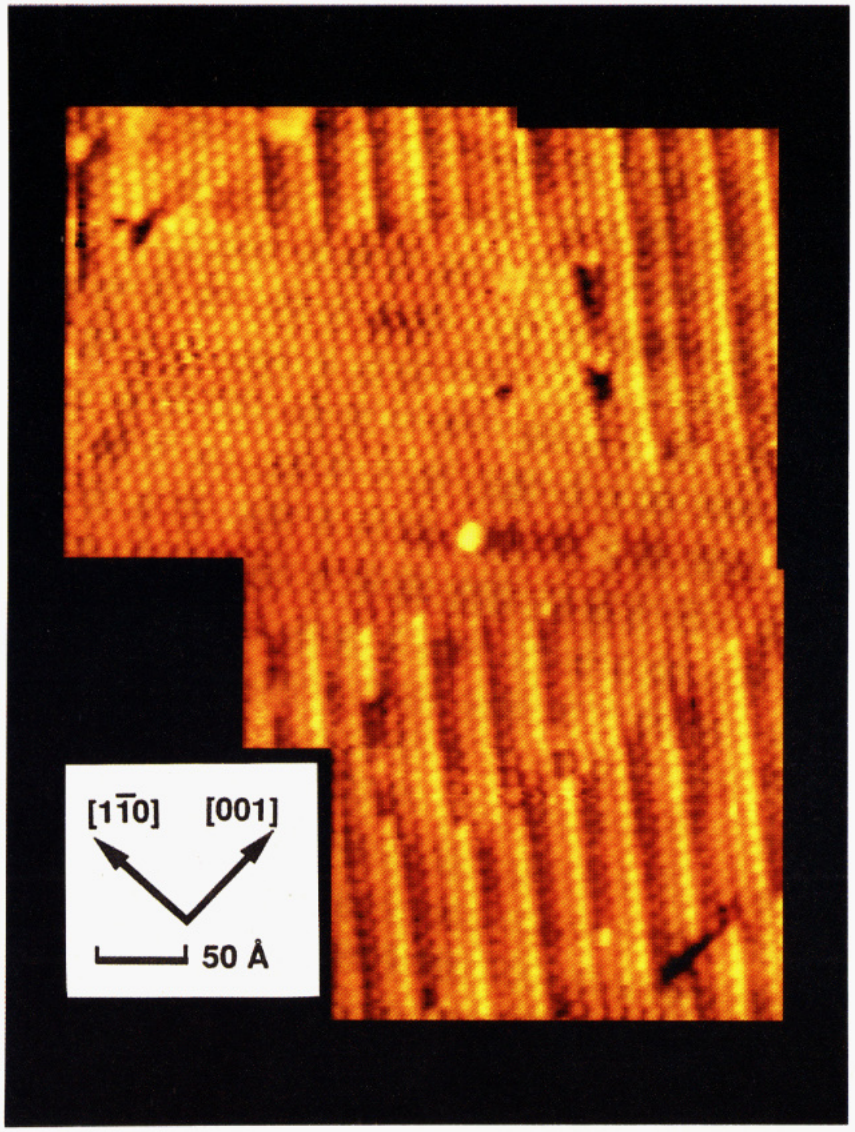

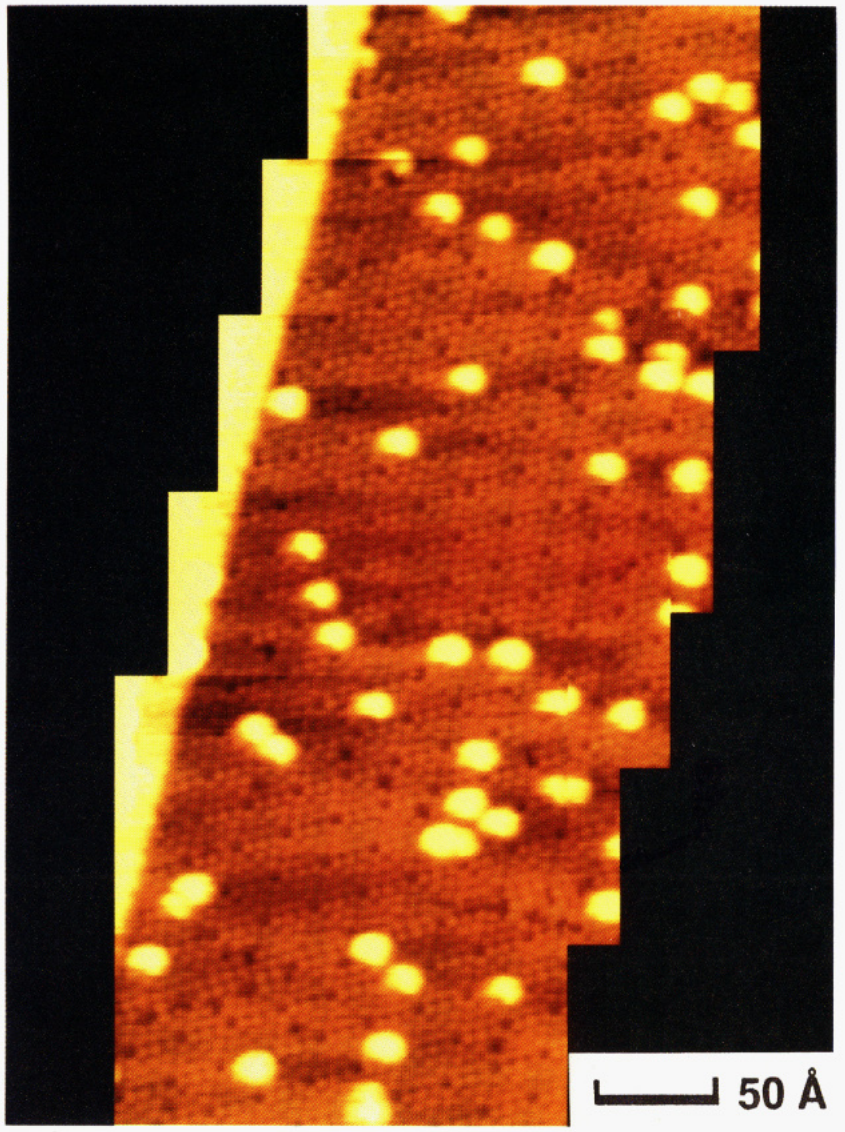

Figure 1. Left (a): STM mosaic for a C_{60} bilayer grown at 450 K on GaAs(110). The flat region in the center reflects the close-packed (111) surface of an fcc crystal. The irregular portions reflect (211) and (533) facets. Right (b): STM mosaic showing isolated C_{60} molecules on a Si(111)-7×7 surface. The bonding appears to be random, and the molecules are stable against repeated scanning. Preferential bonding at the step edge shown at the left is not observed, in contrast to growth on GaAs(110).

below 1×10^{-9} Torr. Fullerene film thicknesses were measured with a quartz crystal thickness monitor. After thorough outgassing, alkali-metal depositions onto the fullerite films could be done at $\sim 2 \times 10^{-10}$ Torr. Stable deposition rates were established prior to exposure to the alkali source.

The Structure of Thin Films: STM Results for C_{60}

Figure 1a is a mosaic of scanning tunneling microscope images for a bilayer of C_{60} grown on GaAs(110) at 450 K.[10] The length scale and substrate orientation are indicated. Each bright feature represents an individual C_{60} molecule, and the intermolecular spacing of ~ 10 Å is consistent with the bulk lattice constant. The central portion shows close-packed molecules defining a (111) surface of the fcc lattice. Close examination of the corrugated regions at the top and bottom shows sawtooth-like structures comprising a mixture of (211) and (533) facets of the fcc structure. The equivalent of a low-angle grain boundary is evident in the upper-right quadrant. At this grain boundary, produced when the flat region joins the corrugated region, one extra row is inserted after six molecules.

The corrugated structures of Figure 1 would seem energetically costly compared to close-packed (111) faces, but they are common even for growth at temperatures to ~450 K. However, the typical island size is much larger when four- to six-layer C_{60} films are grown at 470 K, and the corrugated regions are strikingly absent.[10] It is likely that the tilted close-packed structure serves to relieve strain in the layer in contact with the surface and defines the template for subsequent structures. Growth at 470 K produces a more uniform first monolayer so that additional layers adopt thermodynamically-favored (111) orientations.

The bonding of C_{60} molecules to GaAs(110) is van der Waals in character, and the preference of one site over another is rather weak. The interaction is stronger at substrate steps, even though an atomic step on GaAs(110) is only ~ 2 Å high, compared to a molecular diameter of ~ 10 Å. The step enhances molecular sticking and acts as a nucleation site for islands that grow outward from the steps. When a full layer has formed, the offset for molecules on the upper and lower terraces is clearly evident as a structural discontinuity. This kind of growth pattern may ultimately be useful in fabricating thin film fullerite structures.

STM has also been used to explore the nucleation of multilayers of C_{60}, finding that islands form and then grow together, creating small, two-dimensionally ordered regions and the two-dimensional equivalent of grain boundaries. It is not known if these boundaries propagate through the film layers, but the presence of such complex structures would be detrimental to electron transport and superconductivity and would influence other properties as well.

Surface migration and island formation has been observed for C_{60} on GaAs(110) (refs 9 and 10) and Au(111) (ref 12), but C_{60} molecules stay in isolated sites on the Si(111)-7×7 surface,[13] as shown in Figure 1b for growth at 300 K. The background reflects the 7×7 lattice, and each bright feature corresponds to a C_{60} molecule. This reduced surface migration indicates stronger surface bonding. Analysis reveals approximately equal numbers of C_{60} on faulted and unfaulted halves of the 7×7 unit cell and a range of adsorption sites. Differences in bonding configurations have been identified using bias-dependent imaging and current-imaging tunneling spectroscopy, and these reflect differences in the coupling of electronic states of C_{60} with the substrate Si atoms.

In a series of measurements for C_{60} on Si(111)-7×7, we found that C_{60} could be transferred from the surface to the tip and back again by manipulation of the biasing conditions. Likewise, molecules could be moved laterally on the surface with the tip. This control raises the possibility of patterning the surface with C_{60} molecules, taking advantage of their high stability on Si at 300 K.

Finally, there has been the lingering hope that STM could image individual carbon atoms. This has been frustrated by the fact that molecules in condensed multilayer layers are spinning. Perhaps they can be locked into distinct orientations by condensation on surfaces, but an unambiguous image of pentagons and hexagons has not been obtained. Indeed, it may be that such images will never be obtained because of the complexity of the HOMO and LUMO orbitals and the electronic convolution with the states of the tip.

The Electronic States of Fullerites

Valence and Conduction Bands. Figure 2 summarizes experimental results for the electronic states of condensed C_{60}. The processes associated with photoemission and inverse photoemission are depicted at the top, showing electron removal and electron addition. The photoemission spectra were acquired using monochromatized radiation from the Aladdin synchrotron radiation source. For the inverse photoemission studies, a monoenergetic beam of electrons of energy E_i was focused onto the sample and the energy distribution of the emitted photons was measured.[4] This process corresponds to the radiative decay of electrons from states at energy E_i to lower-lying empty states.

The bottom curves of Figure 2 show the density of states of solid C_{60} calculated using soft pseudopotentials in the local density approximation.[3-5] The theoretical spectrum was convoluted with a Gaussian of width 0.23 eV + $0.2|\Delta E|$ to simulate experimental resolution and lifetime effects. ΔE is the binding energy with respect to the highest occupied or lowest empty level.

Photoemission and inverse photoemission are time-reversed processes in an independent-particle picture, each involving electronic transitions between states coupled by the photon field. In that picture, the two sets of spectra would yield the distribution of occupied and empty states, with a gap evident for a semiconductor. For a molecular solid such as C_{60}, however, the energy-level spectrum also includes effects related to the screening of the $(n - 1)$ and $(n + 1)$ electronic systems. To a first approximation, screening effects can be taken to be equivalent for electrons removed from any of the occupied levels (photoemission) or added to any of the empty levels (inverse photoemission). Hence, the energy scales of Figure 2 are quantitatively meaningful when referenced to the center of the bands derived from the highest occupied or lowest unoccupied

(12) Wilson, R. J.; Meijer, G.; Bethune, D. S.; Johnson, R. D.; Chamblis, D. D.; deVries, M. S.; Hunziker, H. E.; Wendt, H. R. *Nature* **1990**, *348*, 621.
(13) Li, Y. Z.; Chander, M.; Patrin, J. C.; Weaver, J. H. Unpublished.

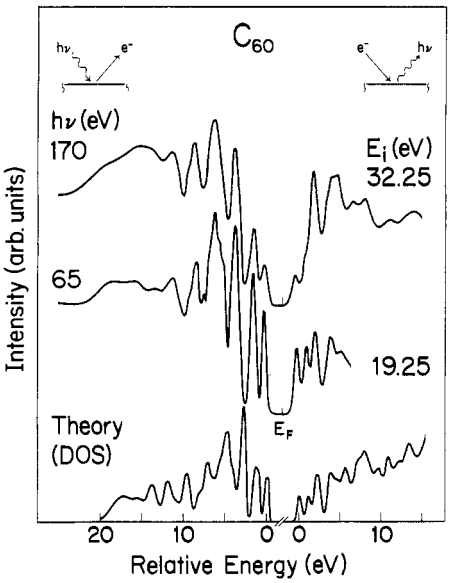

Figure 2. Photoemission and inverse photoemission results showing the distribution of occupied and empty electronic states, referenced in energy to the Fermi level. The theoretical density of states shown at the bottom is referenced to the feature nearest E_F.

molecular levels, HOMO and LUMO, as shown.

Figure 2 shows a gap between the occupied and empty states of solid C_{60}, as expected for a solid derived from closed-shell molecules. For an isolated molecule, the energy separation between HOMO and LUMO would be the difference between the ionization potential and the electron affinity. This is ~5 eV for isolated C_{60}.[14,15] In the solid state, the separation converges to the independent particle gap as screening effects become negligible. For C_{60}, however, that condition is never met, and the measured gap is larger than the ground-state gap by an amount that is a measure of the electron correlation energy.

In the experiments, the Fermi level of the spectrometer, E_F, serves as a direct energy reference. In Figure 2, E_F is 2.25 eV above the center of the HOMO-derived band and 1.5 eV below the center of the LUMO-derived band. The center-to-center separation of 3.8 eV compares to ~1.7 eV for photoemission for C_{60}^- in the gas phase[15] of 1.6 eV for photoemission from the fulleride K_6C_{60}, a solid characterized by complete occupation of the LUMO level.[7,8] The differences are due primarily to screening, and they tell us a great deal about how to think about the electronic properties of these molecular solids.

The experimental results of Figure 2 show line-shape changes as a function of incident photon or electron energy because photoemission and inverse photoemission produce spectra that replicate the density of states modulated by dipole matrix elements. In Figure 2, the empty-state spectra have been normalized so as to give a value of 0.6 for the ratio of LUMO to HOMO peaks. This reflects the theoretical 10-fold degeneracy of the HOMO band and the 6-fold degeneracy of LUMO.[16]

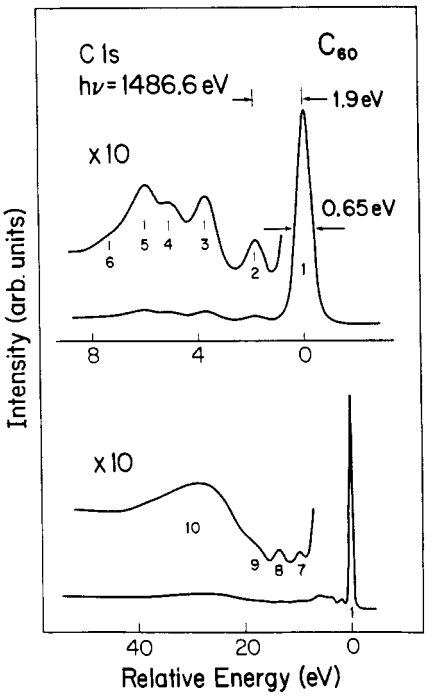

Figure 3. C 1s features for C_{60} showing the main line and a series of loss features that reflect on-site shake-up structures (labeled 2, 3, 7, and 8), dipole energy losses due to scattering of outgoing photoelectrons (3, 4, and 5), and plasmon losses due to collective excitations of the charge of individual molecules (6 and 10).

Analysis of the angular momentum character of the valence states shows that the C $2p_\pi$ levels fall within ~5 eV of E_F, the $2p_\sigma$ levels are concentrated between ~5 and ~10 eV, and the deeper states are derived from 2s-derived σ bands.[3,5,16] The experimental spectra reflect this angular momentum character via changes in photoionization cross sections: p states dominate at low energy, and s states are stronger at higher energy.[3] Significantly, the overall valence-band widths for C_{60}, graphite, and diamond are essentially the same,[17] ~23 eV. Solid C_{60} exhibits much more detailed structure because of the higher symmetry of the molecule and the molecular character in the state density.

The empty-state spectra of Figure 2 show a richness of distinct features within 15 eV of the LUMO-derived band. Analysis shows that states more than ~3 eV above the LUMO are not confined to the molecule but extend throughout the crystal and have band dispersion. Additional evidence for band dispersion comes from comparison of the measured energies of the first three features of the conduction band to calculated energies for isolated molecules and solid C_{60}. Agreement is substantially better in the latter case.[4] Feature 1 has odd symmetry (π-t_u), feature 2 has even symmetry (π-t_g), and feature 3 has contributions from both as well as free-electron character.

For the fullerites, the comparison of theory and experiment is excellent for the electronic states, supporting the truncated icosahedron model. It is gratifying to note the ability to predict states well above the Fermi level for a solid derived from such a large, albeit symmetric, molecule. Such agreement gives us a high level of confidence for calculations of other properties

(14) Lichtenberger, D. L.; Jatcko, M. E.; Nebesny, K. W.; Ray, C. D.; Huffman, D. R.; Lamb, L. D. *Mater. Res. Soc. Symp. Proc.* **1991**, *206*, 673.
(15) Haufler, R. E.; Wang, L.-S.; Chibante, L. P. F.; Jin, C.; Conceicao, J. J.; Chai, Y.; Smalley, R. E. *Chem. Phys. Lett.* **1991**, *179*, 449.
(16) See, for example: Satpathy, S. *Chem. Phys. Lett.* **1986**, *130*, 545. Haddon, R. C.; Brus, L. E.; Ragavachari, K. *Chem. Phys. Lett.* **1986**, *125*, 459.
(17) McFeely, F. R.; Kowalczyk, S. P.; Ley, L.; Cavell, R. G.; Pollack, R. A.; Shirley, D. A. *Phys. Rev.* **1974**, *B9*, 5268. Bianconi, A.; Hagström, S. B. M.; Bachrach, R. Z. *Phys. Rev.* **1977**, *B16*, 5543.

of fullerites and, subsequently, fullerides.

Shake-Up, Energy Loss, and Plasmon Features. Figure 3 shows the C 1s core level emission referenced in energy to the main line for a fullerite film formed at 300 K. The satellite structures, labeled 2–10, are due to on-site and off-site π–π^* excitations and to plasmon losses. (On-site processes are those that occur on the molecule from which the photoelectron is ejected.) The shake-up peak labeled 2 is a result of excitations from HOMO to LUMO states of the molecule induced by the sudden creation of the core hole. This molecular HOMO–LUMO transition is monopole-allowed and is a likely candidate to appear as a shake-up satellite. It is dipole-forbidden for an isolated C_{60} molecule, but solid-state effects mix the angular momentum quantum number. For this reason, the lowest energy transitions in optical spectroscopy occur at about this energy[2,18] and reflect weakly-allowed HOMO–LUMO excitations. From the photoemission–inverse photoemission results, processes related to the creation and separation of an electron–hole pair require screening of the separated particles, and this is not possible for threshold (molecular) excitations. Instead, the electron and the hole are retained on the molecule and decay by direct recombination. Photoenhanced conductance should only be important when there is sufficient energy for electron–hole separation.

The satellite features labeled 3, 4, and 5 originate from π–π^* transitions, but their prominence in electron energy loss spectra (EELS)[19] suggests that they are due to dipole-allowed transitions. Such excitations occur as the photoelectron propagates through the lattice. This interpretation is supported by the agreement between the optical conductivity derived from EELS data[119] and optical absorption measurements.[18] Moreover, the optical spectra for C_{60} in solution and C_{60} films give nearly identical results, supporting the assertion that these excitations are of molecular character, influenced only slightly by solid-state processes. The satellite feature labeled 3 is probably enhanced by monopole-allowed transitions involving HOMO-derived states and empty t_{1u}-derived states. The EELS experiments[19] indicate that the peak at ~6 eV results from both π–π^* transitions at 5.5 and 5.8 eV and the excitation of a π-plasmon at 6.3 eV.

The lower panel of Figure 3 shows two structures, labeled 7 and 8, that are due to monopole-allowed σ–σ^* and σ–π^* transitions and a broad plasmon feature centered ~28 eV below the main line.[3] This feature and the π-plasmon at 6.3 eV are particularly intriguing because equivalent structures are not observed in small molecules. Both are due to collective excitations of the electrons of the molecule, representing the normal modes of a spherical shell of charge. To our knowledge, C_{60} is the first molecule to display a molecular plasmon. It is affected only slightly by changes in the fullerene environment.

C_{60} Bonding and Impurity Levels. Photoemission studies have revealed that first-layer C_{60} bonding to metal and semiconductor surfaces is more than simply van der Waals in character.[20] C_{60} films establish the Fermi level of the substrate as the common energy reference rather than the vacuum level, and this requires the creation of a dipole layer to compensate for differences in work functions. Such dipoles reflect mixing of the empty π states of the molecules with states of the substrate, yielding a π-resonance. For growth on n-type GaAs(110), the dipole involves ~0.02 e/molecule so that the energy levels of the fullerenes are not significantly perturbed.[20] In this case, the spectral features for condensed monolayers are indistinguishable from those for multilayers. For growth on metal surfaces where more charge transfer is involved, a few layers are needed before the influence of the substrate is negligible.[20]

Despite the potential structural complexity of vapor-deposited films, as evident from STM,[10] photoemission measurements from different laboratories have given nearly indistinguishable results for C_{60} when account is taken of resolution or photon energy.[3,7,21] The insensitivity to surface and bulk imperfections indicates the absence of localized energy levels that would produce Fermi level pinning near the band edges. This is consitent with the closed-shell character of C_{60} and the largely-molecular properties of fullerene-derived solids. Although clean fullerene films give remarkably consistent photoemission results, films grown when the fullerene sources are not carefully outgassed exhibited spectral broadening and shifts that reflect Fermi level alignment with states near the bottom of the conduction band derived from the LUMO level of C_{60}.[8]

Alkali-Metal Fullerides

Other contributions to this issue explore the consequences of exposure of C_{60} films to alkali-metal atoms, demonstrating enhanced conductivity, superconductivity in some cases, and compound formation.[22-25] The changes in the electronic properties induced by alkali incorporation are readily evident in spectroscopic studies, as well as in STM studies of K_3C_{60} crystallites.[10] To a significant extent, the picture in which charge is formally donated to C_{60} from alkali atoms housed at interstitial sites is accurate, at least for K and Rb.[26]

(18) Skumanich, A. *Chem. Phys. Lett.* **1991**, *182*, 486. Hebard, A. F.; Haddon, R. C.; Fleming, R. M.; Kortan, A. R. *Appl. Phys. Lett.* **1991**, *59*, 2109. Ren, S. L.; Wang, Y.; Rao, A. M.; McRae, E.; Holden, J. M.; Hager, T.; Wang, K.-A.; Lee, W.-T.; Ni, H. F.; Selegue, J.; Eklund, P. C. *Appl. Phys. Lett.* **1991**, *59*, 2678. Hare, J. P.; Kroto, H. W.; Taylor, R. *Chem. Phys. Lett.* **1991**, *177*, 394. Ajie, H.; Alvarez, M. M.; Anz, S. J.; Beck, R. D.; Diederich, F.; Fostiropoulos, K.; Huffman, D. R.; Krätschmer, W.; Rubin, Y.; Schriver, K. E.; Sensharma, K.; Whetten, R. L. *J. Phys. Chem.* **1990**, *94*, 8630.

(19) Gensterblum, G.; Pireaux, J. J.; Thiry, P. A.; Caudano, R.; Vigneron, J. P.; Lambin, Ph.; Lucas, A. A.; Krätschmer, W. *Phys. Rev. Lett.* **1991**, *67*, 2171. Sohmen, E.; Fink, J.; Krätschmer, W. *Europhys. Lett.*, inp ress. Kuzuo, R.; Terauchi, M.; Tanaka, M.; Saito, Y.; Shinohara, H. *Jpn. J. Appl. Phys.*, in press.

(20) Ohno, T. R.; Chen, Y.; Harvey, S. E.; Kroll, G. H.; Weaver, J. H.; Haufler, R. E.; Smalley, R. E. *Phys. Rev.* **1991**, *44*, 13747.

(21) Chen, C. T.; Tjeng, L. H.; Rudolf, P.; Meigs, G.; Rowe, J. E.; Chen, J.; McCauley, J. P.; Smith, A. B.; McGhie, A. R.; Romanow, W. J.; Plummer, E. W. *Nature* **1991**, *352*, 603.

(22) Haddon, R. C.; Hebard, A. F.; Rosseinsky, M. J.; Murphy, D. W.; Duclos, S. J.; Lyons, K. B.; Miller, B.; Rosamilia, J. M.; Fleming, R. M.; Kortan, A. R.; Glarum, S. H.; Makhija, A. V.; Muller, A. J.; Eick, R. H.; Zahurak, S. M.; Tycko, R.; Dabbagh, G.; Thiel, F. A. *Nature* **1991**, *350*, 320. See Robert Haddon's Account in this issue for more detailed references.

(23) Hebard, A. F.; Rosseinsky, M. J.; Haddon, R. C.; Murphy, D. W.; Glarum, S. H.; Palstra, T. T. M.; Ramirez, A. P.; Kortan, A. R. *Nature* **1991**, *350*, 660.

(24) Zhou, O.; Fischer, J. E.; Coustel, N.; Kycia, S.; Zhu, Q.; McGhie, A. R.; Romanow, W. J.; McCauley, J. P.; Smith, A. B.; Cox, D. E. *Nature* **1991**, *351*, 462. See the Account by Fischer et al. in this issue for more detailed references.

(25) Fleming, R. M.; Ramirez, A. P.; Rosseinsky, M. J.; Murphy, D. W.; Haddon, R. C.; Zahurak, S. M.; Makhija, A. V. *Nature* **1991**, *352*, 787.

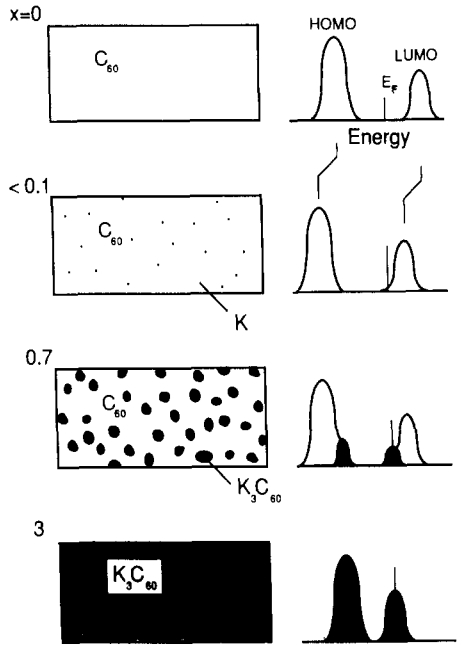

Figure 4. Schematic of the morphology of a K_xC_{60} thin film. The positions of the HOMO- and LUMO-derived bands are shown in relation to E_F. For C_{60}, E_F lies near the middle of the gap. Dilute doping pins E_F near the edge of LUMO. Small K_3C_{60} grains nucleate, probably in grain boundaries or at imperfections in the film. For K_3C_{60}, the Fermi level lies within the LUMO-derived band. Continued incorporation results in polycrystalline K_3C_{60}.

The picture is more complex for the smaller Li and Na ions, where there remains uncertainty about the sites occupied and the structure. For Li and Na, incorporation does not lead to metallic phases such as observed for K and Rb.

Figure 4 depicts different stages of K incorporation in a fullerite film, together with the HOMO and LUMO spectral features. Grain boundaries and other structural irregularities are not shown. The Fermi level lies between the LUMO- and HOMO-derived bands for pure C_{60} (top right of Figure 4). K doping produces a dilute solid solution. These K atoms form bonds with surrounding C_{60} molecules, establishing new energy levels derived mainly from the LUMO levels. These levels pin E_F close to the LUMO band, as sketched. Phase separation occurs when the K concentration exceeds the solubility limit. The work by Fischer et al.[24] and Fleming et al.[25] has shown the resulting K_3C_{60} phase to be a line compound.

The low solubility of K suggests that K_3C_{60} nucleation would occur preferentially at the surface, not in the interior of a single crystal of C_{60}. In thin film samples, imperfections provide channels for easy diffusion and sites for nucleation. The characterization by Hebard et al.[18] of films produced by vapor condensation suggests C_{60} grains of ~60-Å dimension. Calculations have indicated energy gains of 0.5 eV/atom for K in octahedral sites for K_1C_{60}, 0.8 eV/atom for K in tetrahedral sites of K_2C_{60}, and 1 eV/atom for occupancy of tetrahedral and octahedral sites in K_3C_{60}.[7,26] These energies are calculated relative to the standard states for K and C_{60}, and the KC_{60} and K_2C_{60} phases are hypothetical structures.

The third panel of Figure 4 depicts the formation of K_3C_{60} grains and grain growth. For two-phase samples,

(26) Martins, J. L.; Troullier, N. *Phys. Rev. B.* Submitted.

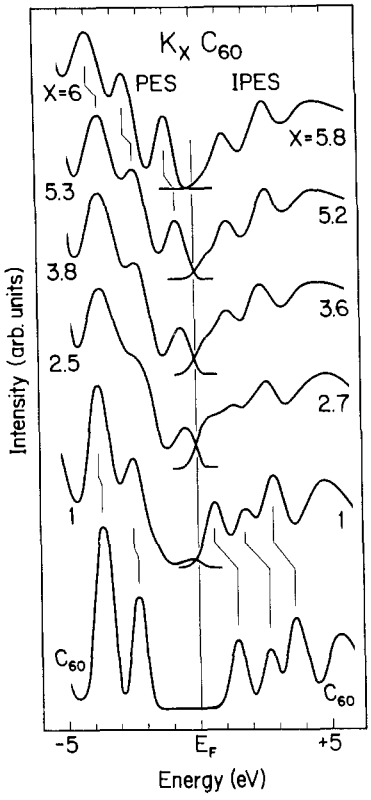

Figure 5. Spectra showing the effects of K incorporation in C_{60} films. The $x = 1$ spectra show emission at E_F from grains of K_3C_{60}. Adding K results in an increase of emission below E_F and a decrease of intensity above E_F. The top spectra show that E_F shifts into the gap when the LUMO bands are filled.

the spectral features of both phases will be present and the sample will resemble a granular metal. Ultimately, the grains form a continuous film with microstructures that reflect the growth conditions and the structure of the starting film. Additional K incorporation produces K_4C_{60} and K_6C_{60} phases with ions in the tetrahedral sites of the bcc C_{60} lattice.[24,25] The K_6C_{60} phase is insulating,[7] but the Fermi level is pinned by holes near the top of the (old) LUMO-derived band for K-deficient K_6C_{60}.[8]

Figure 5 summarizes photoemission and inverse photoemission results for K-incorporated C_{60}.[8] In this case, the photoemission spectra were normalized to keep the HOMO intensity constant, and the IPES spectra were normalized to the height of the third feature. The PES and IPES data were then reconciled by setting the intensity of the LUMO feature in the IPES data to $^3/_5$ the intensity of the HOMO feature for the pure film.

The valence- and conduction-band spectra in Figure 5 provide evidence that filling of LUMO-derived bands with electrons donated from alkali-metal atoms does not result in simple rigid band shifts. This is particularly evident in the empty states because the separation between the LUMO + 1 and LUMO + 2 features changes. The differences reflect a modification in the underlying density of states. The broadening observed in Figure 5 is a combination of several processes, including structural disorder related to grain boundaries and imperfections and differences in local bonding configurations in mixed-phase samples.

Figure 5 shows that the LUMO band shifts away from E_F when it is fully occupied at $x = 6$. This implies that the solid forms the local structure needed to fill

the LUMO-derived molecular states of C_{60}. Were this not the case, E_F would be pinned at the top of the LUMO band in a fashion equivalent to that discussed for $K_{0.1}C_{60}$. The IPES spectra of Figure 5 demonstrate such pinning for x slightly below 6. The fact that an insulating state is reached with E_F in the gap of the (new) molecular solid implies that structural imperfections do not introduce levels that can pin E_F near the band edges. No evidence was found for the filling of the LUMO + 1 band upon further K exposure, but K did condense on the surface.

The results for K_xC_{60} show metallic behavior with the Fermi level falling within the LUMO-derived band for $x \cong 3$. Haddon et al.[22] had showed enhanced conductivity with intermediate doping, and Hebard et al.[23] showed superconductivity with $T_c \cong 18$ K for K_3C_{60}. These remarkable observations stimulated many groups to examine the mechanism of superconductivity from a theoretical point of view. While a review is beyond the scope of this paper, several points should be noted. First, superconductivity had been observed in alkali-intercalated graphite, but the values of T_c were quite low. Second, the phonon spectra for the fullerides is comparable to that of graphite, with phonon modes extending to 0.2 eV. Third, the densities of states of the fullerides and the intercalated graphite compounds are comparable near E_F. Martins et al.[27] suggested that the differences in T_c could be explained by enhanced electron–phonon coupling in the fullerides, an effect related to hybridization of s and p states for the fullerenes.

Very recent photoemission and inverse photoemission studies of the Li and Na fullerides[28] have shown that doping produces phases that are not metallic. In particular, Li and Na fullerides of the form A_2C_{60} were characterized by a band of states completely below E_F that was induced by the alkali atoms. Doping to saturation produced insulating A_6C_{60} phases that were spectroscopically indistinguishable from the saturated K or Rb phases.

The observation of the A_2C_{60} phases raises the question of whether they are band insulators or their character is due to electron correlation effects. The experimental spectra are consistent with the transfer of charge to the 3-fold-degenerate LUMO-derived states of C_{60}, and local density calculations also find charge transfer.[26] Since the calculated band structures of C_{60} and K_3C_{60} show only a shift of the LUMO-derived states with alloying,[26] a large crystal field splitting of those levels in Li_2C_{60} and Na_2C_{60} appears unlikely. Indeed, if the Li and Na atoms occupy the tetrahedral interstices of an fcc crystal, such splitting is ruled out by group theory arguments. On the other hand, there are several indications that the alkali fullerides have strongly correlated electrons and could be close to the metal–insulator transition. First, the measured conductivities of the fullerides[22] are quite low and the mean free paths derived from those values are a few angstroms. Mean free paths close to the C_{60}–C_{60} intermolecular distance are an indication of proximity to a metal–insulator transition.[29] Another measure is the magnitude of the electron–electron interaction parameter, as noted above. Finally, the occupied bandwidth of Rb_3C_{60} (ref 28) and K_3C_{60} (refs 7 and 8) is $\sim$1 eV, much larger than the calculated total bandwidth of $\sim$0.5 eV or the observed width of the peaks of the LUMO-derived states in the insulating phases (Figure 5). This is hard to reconcile with a rigid band picture.

Concluding Remarks

This paper has focused on the electronic interactions of C_{60}, showing the wealth of electronic structure features, noting their origin, and pointing out the gratifying agreement of theory with experiment. We have tried to urge caution when considering the optical properties and transport properties based on independent-particle electron calculations because of the importance of many-body effects. The surface structures observed for isolated C_{60} on Si and for C_{60} thin films have been shown through STM imaging.

It is now accepted that C_{60} forms a molecular solid and that the highest valence and lowest conduction bands are quite narrow. It is remarkable that compounds of C_{60} with the different alkali metals can exhibit metallic and insulating character. This narrow-band character is certain to be important in solid-state processes for other fullerides, and it is likely to be important for fullerides based on the higher fullerenes.

Recent advances in the synthesis of endofullerenes[30] and fullerenes with other elements substituted in the cage assure that there will be rapid advances in solid-state studies of these species and compounds derived from them. Spectroscopic information will play an important role in understanding the electronic interactions in these exciting new materials.

This work was done in collaboration with P. J. Benning, M. Chander, Y. Chen, C. Gu, M. B. Jost, G. H. Kroll, Y. Z. Li, J. L. Martins, T. R. Ohno, J. C. Patrin, D. M. Poirier, F. Stepniak, and N. Troullier at the University of Minnesota and L. P. F. Chibante, R. E. Haufler, J. Fure, and R. E. Smalley at Rice University. The work discussed here was supported by the National Science Foundation, the Office of Naval Research, and the Robert A. Welch Foundation (Rice).

(27) Martins, J. L.; Schabel, M. C.; Troullier, N. Unpublished.

(28) Gu, C.; Stepniak, F.; Poirier, D. M.; Jost, M. B.; Benning, P. J.; Chen, Y.; Ohno, T. R.; Martins, J. L.; Weaver, J. H.; Fure, J.; Smalley, R. E. *Phys. Rev. B*, in press.

(29) Mott, N. F. *Metal Insulator Transitions*; Taylor & Francis: London, 1990.

(30) Chai, Y.; Guo, T.; Jin, C.; Haufler, R. E.; Chibante, L. P. F.; Fure, J.; Wang, L.; Alford, J. M.; Smalley, R. E. *J. Phys. Chem.* **1991**, *95*, 7564. Weaver, J. H.; Chai, Y.; Kroll, G. H.; Jin, C.; Ohno, T. R.; Haufler, R. E.; Guo, T.; Alford, J. M.; Conceicao, J.; Chibante, L. P. F.; Jain, A.; Palmer, G.; Smalley, R. E. *Chem. Phys. Lett.*, in press.